Efficiency and power of a thermoelectric quantum dot device

D.M. Kennes, D. Schuricht and V. Meden

Institut für Theorie der Statistischen Physik and JARA—Fundamentals of Future Information Technology, RWTH Aachen University, 52056 Aachen, Germany

PACS 73.50.Lw – Thermoelectric effects
PACS 05.60.Gg – Quantum transport
PACS 73.63.Kv – Electronic transport in nanoscale materials and structures: QD

Abstract –We study linear response and nonequilibrium steady-state thermoelectric transport through a single-level quantum dot tunnel coupled to two reservoirs held at different temperatures as well as chemical potentials. A fermion occupying the dot interacts with those in the reservoirs by a short-ranged two-particle interaction. For parameters for which particles flow against a bias voltage from the hot to the cold reservoir this setup acts as an energy-conversion device with which electrical energy is gained out of waste heat. We investigate how correlations affect its efficiency and output power. In linear response the changes in the thermoelectric properties can be traced back to the interaction induced renormalization of the resonance line shape. In particular, small to intermediate repulsive interactions reduce the maximum efficiency. In nonequilibrium the situation is more complex and we identify a parameter regime in which for a fixed lower bound of the output power the efficiency increases.

Introduction. – Quantum dots (QDs) are considered as high-potential solid-state energy conversion devices to gain electrical energy out of waste heat [1]. In a minimal setup electrons from a hot right reservoir (at temperature T_R) are transported via a weakly coupled QD to a cold left one (at T_L) against a bias voltage $V = \mu_L - \mu_R \geq 0$. Here μ_α denotes the chemical potential of reservoir $\alpha = L, R$ and we use units in which the elementary charge $e = 1$. Within *linear response*, that is for small temperature differences and small bias voltages, one aims at a high efficiency η of energy conversion. It is defined as $\eta = P/|I_\mathrm{h}|$, with the output power $P = V|I_\mathrm{c}|$ and the charge/heat currents $I_{\mathrm{c/h}}$ [2]. As a measure of η in QD setups one often uses the so-called figure of merit ZT [1]; the larger ZT the closer η comes to its upper bound, the Carnot efficiency η_C. We here neglect the contribution of the phonon thermal conductance to ZT and focus on the electronic degrees of freedom. The figure of merit is inversely proportional to the Lorenz number. Under the assumption of scattering processes which on the scale $T_R \approx T_L \approx T$ only weakly depend on energy the Wiedemann-Franz law states that the latter is a material independent number. This in turn limits the electronic ZT in bulk materials which obey this law. In QDs due to the strong energy dependence of the transmission close to transport resonances [1, 3, 4] the Wiedemann-Franz law does not apply as long as the temperature is larger than the resonance width Γ. Therefore, in transport through dots with sharp resonances a large figure of merit and thus a high efficiency can be realized [1, 3–5]. Equivalently, QDs can be used as efficient solid-state systems for cooling of nanoelectronic devices [6].

Due to the confinement of electrons in QDs to meso- or nanoscopic regions the local Coulomb interaction becomes a relevant energy scale. This two-particle interaction strongly alters the line shape of resonances and thus the thermoelectric properties [4, 5, 7]. For example, the Kondo effect, resulting from correlated spin fluctuations, leads to a very sharp many-body resonance of width much smaller than the noninteracting Γ. This has crucial consequences for thermoelectric transport [8–14]. Even in the absence of the Kondo effect correlated charge fluctuations affect the line width as was worked out in detail for the interacting resonant level model (IRLM) [15–20]. For weak to intermediate local Coulomb repulsions the interaction renormalized width Γ^ren is increased compared to the noninteracting one Γ, while for strong repulsive interactions as well as attractive ones $\Gamma^\mathrm{ren} < \Gamma$. Effectively attractive interactions might be realized in molecular QDs with strong local electron-phonon coupling [11]. The consequences of the interaction renormalized resonance line shape for the thermoelectric transport properties were not discussed so far. We fill this gap and show that the parameter de-

pendence of η and P can be understood in terms of the line width renormalization. We provide approximate analytical results for the efficiency and the output power which for small two-particle interactions agree very well with numerical data. For weak repulsive interactions the maximum efficiency decreases, it increases for attractive ones. Depending on the temperature regime considered the two-particle interaction can lead to an increase or to a decrease of the power at maximum efficiency.

In linear response the output power is of order ΔT^2, with $\Delta T = T_L - T_R < 0$, and thus small (see below). Depending on the precise technological conditions under which the QD 'heat engine' is supposed to perform (fixed or tunable ΔT, limited or unlimited supply of heat, scalability in parallel or series, etc.) it might be meaningful to maximize P instead of η by varying the model parameters and the voltage at fixed temperatures, with $|\Delta T|$ not necessarily being small. In fact, within the framework of nonequilibrium thermodynamics studying the efficiency at maximum power of general heat engines is an active field of current research [21–27]. In this context the noninteracting resonant level model in the limit of vanishing level-reservoir coupling was studied as a toy model [28]. Even questions such as 'what is the optimal efficiency reachable for the power being larger than a given lower bound' might be of interest. Computing the efficiency at maximum power and answering questions of the above type requires access to the full *nonequilibrium* (in V and ΔT) *steady-state* properties [29]. For microscopic models of QDs with local two-particle correlations achieving this presents a formidable challenge; for a recent review, see e.g. Ref. [30]. In particular, this holds if nonperturbative effects in both the level-reservoir coupling as well as the two-particle interaction become crucial as it is the case in the IRLM [15–20].

Only recently a very flexible nonperturbative tool was developed which allows to treat the full-fledged nonequilibrium steady state of the IRLM [19,31,32] at weak interactions. It is based on Keldysh Green functions [33] and the functional renormalization group approach to quantum many-body physics [34]. Here we apply this method to study the efficiency and power output of the IRLM 'heat engine' beyond linear response. Broadly speaking the effect of the interaction on the efficiency (at maximum power) is similar to the one found in linear response (summarized in the next to last paragraph). By closer inspection we identify a situation in which a weak repulsive interaction can lead to an increase of the efficiency by a few percent at fairly large power output.

We here focus on correlation effects in the elementary two-reservoir IRLM but expect our results to be of relevance for other models showing correlated charge fluctuations as well. Very recently three-terminal systems with the reservoirs having more complex degrees of freedom (e.g. magnetic ones) were identified as promising energy converters [35–37]. In those systems electrons are transported against a bias between two of the reservoirs by extracting heat from the third one.

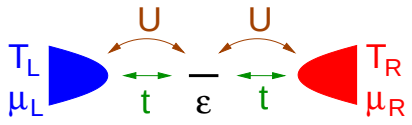

Fig. 1: Sketch of the investigated model.

Quantum dot model. – Our model Hamiltonian sketched in Fig. 1 consists of three parts $H = H_\mathrm{r} + H_\mathrm{d} + H_\mathrm{c}$. The two spinless reservoirs are assumed to be identical and are given by

$$H_\mathrm{r} = \sum_{k,\alpha} \epsilon_k \, c^\dagger_{k,\alpha} c_{k,\alpha}, \tag{1}$$

with fermionic ladder operators $c^{(\dagger)}_{k,\alpha}$, where k denotes a set of quantum numbers characterizing the reservoir states. To disentangle effects of the reservoir band structure encoded in the dispersion ϵ_k and the correlations on the thermoelectric properties we assume structureless reservoirs with an energy independent density of states ρ between $-D$ and D and the bandwidth $2D$ being much larger than any other energy scale. The reservoirs are in grand canonical equilibrium with $T_\alpha = 1/\beta_\alpha$ and chemical potentials centered around zero: $\mu_L = -\mu_R = V/2$ (with $\hbar = k_\mathrm{B} = e = 1$). The dot part of H is given by $H_\mathrm{d} = \epsilon n$, with the dot occupation number operator $n = d^\dagger d$. The energy ϵ of the level is assumed to be tunable; in experiments this is achieved by applying a voltage to a properly fabricated gate. Finally, the coupling reads

$$H_\mathrm{c} = t \sum_{k,\alpha} \left(c^\dagger_{k,\alpha} d + \mathrm{H.c.} \right) + u \left(n - \frac{1}{2} \right) \sum_{k,k',\alpha} {:}c^\dagger_{k,\alpha} c_{k',\alpha}{:}, \tag{2}$$

where $:\ldots:$ denotes normal ordering. This and the shift of the dot occupancy by $-1/2$ ensures that $\epsilon = 0$ corresponds to half dot filling. For simplicity we assume the tunnel couplings to the left and right reservoir t to be equal; similarly for the two-particle interactions u to the left and right. We note that within our approach to the many-body problem these restrictions can easily be relaxed. We use the dimensionless interaction $U = \rho u$.

Thermoelectric transport at $U = 0$. – For $U = 0$ transport through the dot is characterized by a Breit-Wigner transmission resonance

$$\tau(\omega) = \frac{\Gamma^2}{(\omega - \epsilon)^2 + \Gamma^2} \tag{3}$$

of width $\Gamma = 2\pi\rho t^2$. The steady-state charge current I_c (leaving the left reservoir) and heat current I_h (entering the right reservoir) can be computed using the Landauer-Büttiker formalism

$$I_\mathrm{c} = \frac{1}{2\pi} \int d\omega \, \tau(\omega) \left[f_L(\omega) - f_R(\omega) \right], \tag{4}$$

$$I_\mathrm{h} = \frac{1}{2\pi} \int d\omega \, (\omega - \mu_R) \tau(\omega) \left[f_L(\omega) - f_R(\omega) \right], \tag{5}$$

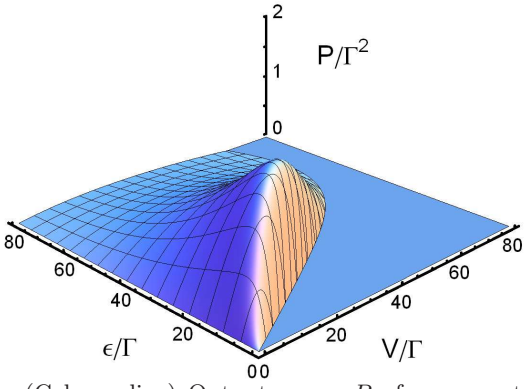

Fig. 2: (Color online) Output power P of our quantum dot device for vanishing two-particle interaction as a function of ϵ/Γ and V/Γ for $T_L/\Gamma = 1$ and $T_R/\Gamma = 20$. Data points are only shown in the regime in which the device acts as a 'heat engine' (curved surface with lines).

with the Fermi functions $f_\alpha(\omega) = \left[e^{(\omega-\mu_\alpha)/T_\alpha}+1\right]^{-1}$. We express the energy integral in I_c in terms of the digamma function $\Psi(0,z)$ as

$$I_\mathrm{c}(\epsilon) = \frac{\Gamma}{2\pi}\,\mathrm{Im}\left[\Psi\left(0,\frac{1}{2}+\frac{i}{2\pi T_R}[\epsilon-\mu_R-i\Gamma]\right)\right.$$
$$\left.-\Psi\left(0,\frac{1}{2}+\frac{i}{2\pi T_L}[\epsilon-\mu_L-i\Gamma]\right)\right] \qquad (6)$$

and the heat current as a sum of the charge current and the Hilbert transform of the latter

$$I_\mathrm{h}(\epsilon) = (\epsilon-\mu_R)I_\mathrm{c}(\epsilon) - \frac{\Gamma}{\pi}\,\mathcal{P}\!\int d\epsilon'\frac{I_\mathrm{c}(\epsilon')}{\epsilon-\epsilon'}. \qquad (7)$$

In Eqs. (6) and (7) Γ can be scaled out (taken as the unit of energy) and η as well as P can be investigated as functions of the model parameter ϵ/Γ, the external bias voltage V/Γ, and $T_{L/R}/\Gamma$. In analogy to studies on periodic heat engines in thermodynamics we assume that $T_{L/R}$ are fixed by the environment. With $|\Delta T|/\Gamma$ not necessarily being small we cannot resile to the linear response regime. Figure 2 shows $P = V|I_\mathrm{c}|$ in the ϵ-V-plane for $T_L/\Gamma = 1$ and $T_R/\Gamma = 20$. It has a unique maximum.

To set the stage for more general considerations we first consider the limit $\Gamma \to 0$ [28]. The second term in Eq. (7) is of higher order in Γ as compared to the first one and can be neglected. As a consequence charge and heat flow are 'perfectly coupled' (proportional to each other); for $\Gamma \to 0$ the energy of every particle coming from the dot level becomes sharp and is fixed at ϵ [28]. For applications it is meaningful to maximize the output power—the maximum is denoted by P_m in the following—and study the efficiency at maximum power η_mp as a function of $T_{L/R}$. The optimization is performed with respect to the level energy ϵ and the externally applied voltage V both being parameters which in experiments on QDs can routinely be varied with high precision. As shown analytically in Ref. [28] for $\Gamma \to 0$, η_mp and P_m are functions of T_L/T_R only and can thus be written as functions of the Carnot efficiency $\eta_\mathrm{C} = 1 - T_L/T_R = |\Delta T|/T_R$.

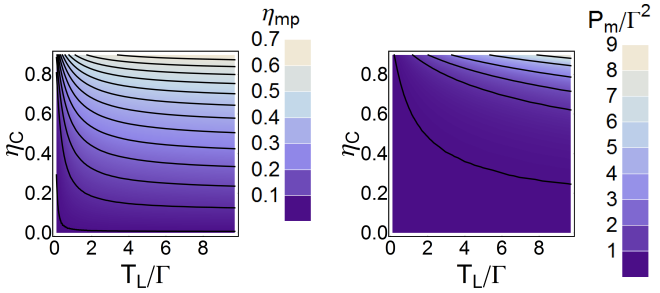

Fig. 3: (Color online) The efficiency at maximum power (left) and the maximum power (right) for $U = 0$ as functions of T_L/Γ and $\eta_\mathrm{C} = 1 - T_L/T_R$. Contour lines are shown.

We now return to $\Gamma > 0$ and numerically maximize the output power with respect to ϵ and V using Eqs. (6) and (7). Both, η_mp and P_m are no longer functions of η_C only. This becomes apparent from Fig. 3 which shows η_mp and P_m as functions of T_L/Γ and η_C. Only in the limit of large T_L/Γ, that is small Γ, the dependence on T_L/Γ drops out. For small T_L/Γ rather large $\eta_\mathrm{C} = |\Delta T|/T_R$ (close to 1) are required to obtain a sizable efficiency at maximum power.

Expanding Eqs. (6) and (7) to lowest order in $\Delta T/\Gamma$ and V/Γ we obtain linear response results [5]. The currents follow from the Onsager matrix containing the conductances

$$\begin{pmatrix} I_\mathrm{c} \\ I_\mathrm{h} \end{pmatrix} = \begin{pmatrix} G_\mathrm{c} & G_\mathrm{c}^{\Delta T} \\ G_\mathrm{h}^{V} & G_\mathrm{h} \end{pmatrix}\begin{pmatrix} V \\ \Delta T \end{pmatrix}. \qquad (8)$$

The Onsager (time-reversal) symmetry gives $G_\mathrm{h}^V = TG_\mathrm{c}^{\Delta T}$, with $T = T_L = T_R$, and the independent matrix elements can be written as [5]

$$G_\mathrm{c} = \frac{\Gamma}{8\pi^2 T}\left[\Psi\left(1,\frac{\pi+w}{2\pi}\right)+\mathrm{c.c.}\right], \qquad (9)$$

$$G_\mathrm{c}^{\Delta T} = -\frac{i\Gamma}{8\pi^2 T}\left[w\Psi\left(1,\frac{\pi+w}{2\pi}\right)-\mathrm{c.c.}\right], \qquad (10)$$

$$G_\mathrm{h} = \frac{\Gamma}{2\pi}\left(\frac{\Gamma}{T}-\frac{1}{4\pi}\left[w^2\Psi\left(1,\frac{\pi+w}{2\pi}\right)+\mathrm{c.c.}\right]\right), \qquad (11)$$

with the trigamma function $\Psi(1,z)$ and $w = (\Gamma + i\epsilon)/T$.

In linear response one aims at a high efficiency. Independent of the model considered on first maximizes $\eta = V|I_\mathrm{c}|/|I_\mathrm{h}|$ with respect to V [22, 25] using Eq. (8) and leading to

$$\eta_0 = \frac{\sqrt{ZT+1}-1}{\sqrt{ZT+1}+1}\,\frac{|\Delta T|}{T}, \quad ZT = \frac{(G_\mathrm{c}^{\Delta T})^2 T}{G_\mathrm{c}G_\mathrm{h} - (G_\mathrm{c}^{\Delta T})^2 T}. \qquad (12)$$

The maximum is reached for a voltage of order ΔT and the linear response regime is not left. Equation (12) constitutes the relation between the efficiency and the figure of merit ZT announced in the introduction; the latter being expressible in terms of the conductances. We can now be more precise: ZT is a measure for the linear response efficiency *maximized with respect to* V. For $ZT \to \infty$, η_0 approaches the linear response Carnot efficiency $|\Delta T|/T$

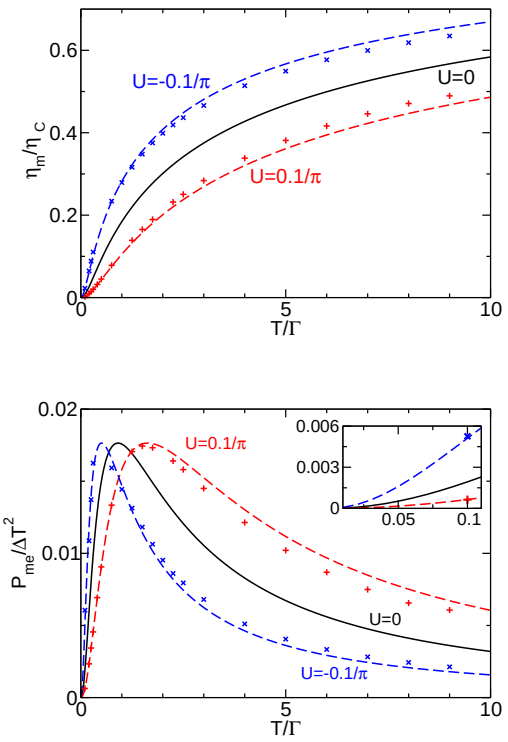

Fig. 4: (Color online) Linear response maximum efficiency (upper panel) and the corresponding output power (lower panel) for different interactions U as functions of T/Γ. The lines follow from Eqs. (8)-(11) and (14) (for $U \neq 0$) while the symbols are numerical data obtained from our many-body approach. Inset: zoom-in of the regime $T/\Gamma \ll 1$.

which constitutes an upper bound for all thermodynamic efficiencies. The power corresponding to η_0 is given by

$$P_0 = \frac{TG_\mathrm{h}}{\sqrt{ZT+1}} \frac{\sqrt{ZT+1}-1}{\sqrt{ZT+1}+1} \left(\frac{\Delta T}{T}\right)^2 \qquad (13)$$

and thus of order $(\Delta T)^2$; one factor ΔT comes from the voltage at which the maximum efficiency is reached and the other from the charge current. In the limit $ZT \to \infty$, with $\eta_0 \to \eta_\mathrm{C}$, the prefactor of P_0 vanishes.

We now return to our specific model and similar to the nonequilibrium case above first consider the limit $\Gamma \to 0$. Independent of $\epsilon \neq 0$ one finds $ZT \sim 1/\Gamma$ [5] and thus $\eta_0 \to \eta_\mathrm{C}$ [28]. Furthermore, $G_\mathrm{h} \sim \Gamma$ and $P_0 \to 0$.

For $\Gamma > 0$ we numerically maximize η_0 (in addition) with respect to ϵ using Eqs. (8)-(11) [5]. The resulting efficiency η_m and power at maximum efficiency P_me as functions of T/Γ are shown in Fig. 4. As discussed above for $\Gamma \to 0$, that is for large T/Γ, η_m approaches Carnot efficiency and $P_\mathrm{me}/\Delta T^2$ vanishes. The latter also vanishes for $T/\Gamma \to 0$ and is thus a nonmonotonic function with a maximum at $T \approx \Gamma$. Our calculations show that for small T the level energy at which optimal efficiency is reached approaches a constant. Using this and the expansions of Eqs. (9)-(11) we obtain $TG_\mathrm{h} \sim T^2$ and $ZT \sim T^2$. Thus $P_\mathrm{me}/\Delta T^2 \sim T^2$ (see the inset of Fig. 4).

Thermoelectric transport at $U \neq 0$. – To investigate the linear response and nonequilibrium steady-state transport properties in the presence of two-particle correlations we use a technique which is based on nonequilibrium Keldysh Green functions [33] and the functional renormalization group approach to quantum many-body physics [34]. In this one derives an exact infinite hierarchy of coupled differential equations for the many-body self-energy and the effective n-particle interactions (one-particle irreducible vertex functions). The derivative is taken with respect to a low-energy cutoff and the set of equations have to be integrated from infinity to zero. Concrete calculations require truncations. We apply the lowest-order approximation in which only the self-energy flow is kept. It was earlier used to study the IRLM for $|U| \ll 1$ in equilibrium as well as the charge current in steady-state nonequilibrium [19, 31, 32]. We refrain from giving any technical details and instead refer the interested reader to Refs. [19] and [32].

As its main effect the two-particle interaction generates a renormalization group flow of the hybridization $\Gamma/2$ to the individual reservoirs. For the left one it is cut off by the largest of the energy scales $|\epsilon - \mu_L|$, T_L, and the total hybridization; for the right one one has to replace the index L by R [19, 31, 32]. This leads to a power-law scaling $\Gamma_\alpha^\mathrm{ren}/\Gamma \sim (s/D)^{-\nu(U)}$, with the corresponding largest scale s (still much smaller than D) and the U-dependent exponent ν. To leading order one finds $\nu(U) = 2U$ [15, 18–20, 31, 32, 38]. This correlation effect cannot be captured by perturbative (in either U or Γ) approaches. In a general nonequilibrium setup $\Gamma_L^\mathrm{ren} \neq \Gamma_R^\mathrm{ren}$ even in the case of equal bare hybridizations. To exemplify how the renormalization manifests in physical observables we consider the linear response ($V, \Delta T \to 0$) charge conductance G_c as a function of ϵ close to the resonance (at $\epsilon = 0$) and $T = 0$ [17, 19, 20]. The largest scale cutting off the renormalization group flow of the hybridizations is given by Γ . Using the above scaling law one concludes that the resonance in G_c has the width

$$\Gamma^\mathrm{ren} = W = \Gamma \left(\frac{2\Gamma}{D}\right)^{-2U}, \qquad (14)$$

which defines the emergent energy scale W. The resonance becomes wider for weak (to intermediate [17]) repulsive interactions but more narrow for attractive ones. To illustrate how Γ^ren changes when two or more of the energy scales are of the same order [19, 31, 32] we consider $T \gtrapprox W$. In this case $\Gamma^\mathrm{ren} \approx W(T/W)^{-2U}$; see Fig. 1 of Ref. [32]. Since $|U| \ll 1$ the correction to W is of order one as long as T does not exceed W by several orders of magnitude. Further down this will become crucial.

We start the discussion of our results of correlation effects on the efficiency and power considering linear response. The symbols in Fig. 4 show the maximum efficiency η_m (maximized with respect to V and ϵ) and

the power at maximum efficiency $P_{\rm me}$ for $U = \pm 0.1/\pi$ obtained by numerically integrating the renormalization group equations and computing the charge and thermal currents [39]. For weak repulsive interactions $\eta_{\rm m}$ is reduced compared to the noninteracting result, while it is increased for weak attractive ones. Depending on the temperature regime considered the interaction enhances or reduces $P_{\rm me}$. These results can be understood analytically by employing the above discussed energy scale dependence renormalization of the resonance width. For $U = 0$ the level energy ϵ at which the maximum efficiency is reached is of the order of a few T at large T [5] while it saturates at a constant of order Γ for small T . This also holds for small $|U|$. Thus Eq. (14) gives a very good estimate of the renormalized hybridization for all temperatures shown in Fig. 4. This motivates us to replace Γ in the noninteracting expressions Eqs. (8)-(11) for the charge and heat currents by W Eq. (14). The corresponding results for $\eta_{\rm m}$ and $P_{\rm me}$ are shown as dashed lines in Fig. 4. As expected they show excellent agreement with the numerical data. The deviations at $T/\Gamma \gtrapprox 1$ are consistent with the finite T correction to W discussed above.

As our approximate approach is restricted to $|U| \ll 1$ we cannot access the regime of large interactions. It is known that $\Gamma^{\rm ren}$ is a nonmonotonic function of $U > 0$ and for large repulsive interactions one finds $\Gamma^{\rm ren} < \Gamma$ [17,18]. This can be explained by the appearance of a second order term $\sim -U^2$ (related to the so-called orthogonality catastrophe) which dominates for $U > 1$ and changes the sign of the exponent ν [18]. Based on our above results it is thus reasonable to assume that for large repulsive interactions η will be increased compared to the noninteracting case. It would be very interesting to explicitely verify this using a method complementary to ours.

We next leave the linear response regime. Figure 5 shows the U dependence of the maximum power $P_{\rm m}$ and the efficiency at maximum power $\eta_{\rm mp}$ for different sets of $T_{L/R}$ obtained numerically using our nonequilibrium many-body method. In analogy to the maximum efficiency in linear response $\eta_{\rm mp}$ is a decreasing function of U. A similar analogy to the linear response results for $P_{\rm me}$ Fig. 4 holds for the maximum power $P_{\rm m}$. It is a decreasing function of U for temperatures $T_{L/R}$ smaller than Γ and an increasing one for $T_{L/R}/\Gamma \gg 1$. For intermediate temperatures we find nonmonotonic behavior. We have also studied the U dependences of the maximum (with respect to V and ϵ) efficiency and the corresponding output power beyond the linear response regime. They are qualitatively similar to the results for $\eta_{\rm mp}$ and $P_{\rm m}$ shown in Fig. 5.

We finally investigate a situation in which even a weak repulsive interaction can lead to an increase of the efficiency. Let us assume that our 'heat engine' has to produce at least a certain minimal output power. This might e.g. be a sensible requirement if we are interested in charging a battery. For appropriate temperatures $T_{L/R}$ the maximum power increases with U (see Fig. 5) and one can hope to overcome the decrease of the efficiency. For

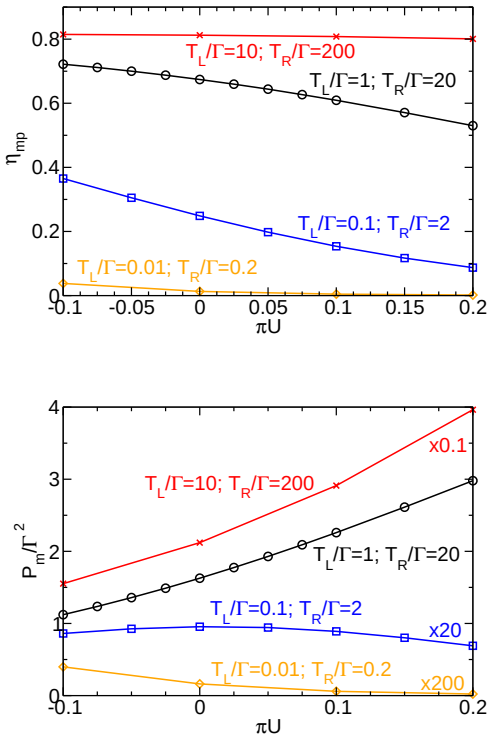

Fig. 5: (Color online) Efficiency at maximum power (upper panel) and the maximum power (lower panel) for different sets of $T_{L/R}$ as functions of U. The lines are guide to the eyes. The data are scaled by the given factors.

fixed $T_{L/R}$ we proceed as follows: as our lower bound of the power $P_{\rm bound}$ we take the maximum power at $U = 0$. This is a convenient choice to reduce the number of parameters. Varying ϵ and V we then search for the largest efficiency $\eta_>$ at fixed $U > 0$ with $P \geq P_{\rm bound}$. As this is a numerically demanding procedure—remind that for every parameter set the currents $I_{\rm c/h}$ have to be computed numerically solving coupled differential flow equations—we restrict ourselves to one of the temperature sets (with increasing power) of Fig. 5 namely $T_L/\Gamma = 1$ and $T_R/\Gamma = 20$. The U dependence of $\eta_>$ is shown in Fig. 6. Under the above requirement one can increase the efficiency by a few percent by turning on a small repulsive interaction.

Summary. – We have discussed the charge and heat transport properties of an elementary single-level quantum dot 'heat engine' which can be used to convert waste heat into electrical energy. Firstly, we have studied the linear response and nonequilibrium steady-state thermoelectric properties in the absence of local Coulomb correlations. The efficiency and output power of this device was investigated in all details. We next included the local two-particle interaction which in meso- or nanoscopic devices is an important energy scale. Using a flexible approximate many-body method which can be applied in equilibrium (linear response) as well as the in the nonequilibrium

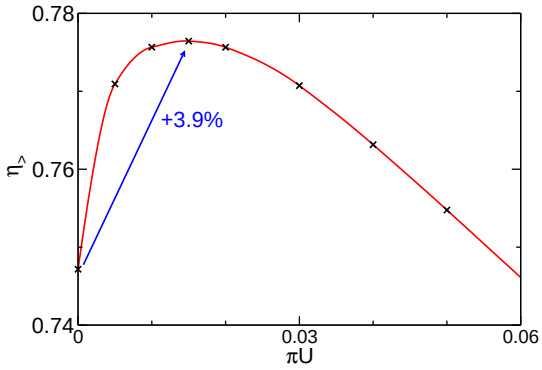

Fig. 6: (Color online) Interaction U dependence of the largest efficiency obtainable with $P \geq P_{\text{bound}}$ for $T_L/\Gamma = 1$ and $T_R/\Gamma = 20$ (for details see the text). The line is an Akima spline interpolating between the computed data points (symbols). The efficiency can be raised by a few percent by turning on a small repulsive interaction.

steady state we were able to present a comprehensive picture of the correlation effects on the efficiency and output power.

* * *

We are grateful to S. Andergassen, C. Van den Broeck, and M. Laakso for enlightening discussions. This work was supported by the DFG via FOR 723 (DK and VM) as well as the Emmy-Noether program (DS).

REFERENCES

[1] Mahan, G.D. and Sofo, J.O., *Proc. Natl. Acad. Sci. USA*, **93** (1996) 7436.
[2] We are only interested in the part of the parameter space in which our setup can be used to gain electrical energy. We thus define η and P such that both are positive under this condition (absolute values of the currents).
[3] Mahan, G.D., Sales, B. and Sharp, J., *Phys. Today*, **50** (1997) 42.
[4] Kubala, B., König, J. and Pekola, J., *Phys. Rev. Lett.*, **100** (2008) 066801.
[5] Murphy, P., Mukerjee, S. and Moore, J., *Phys. Rev. B*, **78** (2008) 161406(R).
[6] Giazotto, F., Heikkilä, T.T., Luukanen, A., Savin, A.M. and Pekola, J.P., *Rev. Mod. Phys.*, **78** (2006) 217.
[7] Kubala, B. and König, J., *Phys. Rev. B*, **73** (2006) 195316.
[8] Kim, T.-S. and Hershfield, S., *Phys. Rev. B*, **67** (2003) 165313.
[9] Scheibner, R., Buhmann, H., Reuter, D., Kiselev, M.N. and Molenkamp, L.W., *Phys. Rev. Lett.*, **95** (2005) 176602.
[10] Costi, T.A. and Zlatić, V., *Phys. Rev. B*, **81** (2010) 235127.
[11] Andergassen, S., Costi, T.A. and Zlatić, V., *Phys. Rev. B*, **84** (2011) 241107(R).
[12] Rejec, T., Žitko, R., Mravlje, J. and Ramšak, A., *Phys. Rev. B*, **85** (2012) 085117.
[13] Roura-Bas, P., Tosi, L., Aligia, A.A. and Cornaglia, P.S., *Phys. Rev. B*, **86** (2012) 165106.
[14] Hong, S., Ghaemi, P., Moore, J.E. and Phillips, P.W., arXiv:1301.1441.
[15] Schlottmann, P., *Phys. Rev. B*, **22** (1980) 613; *Phys. Rev. B*, **25** (1982) 4815.
[16] Filyov, V.M., Tzvelik, A.M. and Wiegmann, P.B., *Phys. Lett.*, **81A** (1980) 175.
[17] Bohr, D. and Schmitteckert, P., *Phys. Rev. B*, **75** (2007) 241103.
[18] Borda, L., Vladár, K. and Zawadowski, A., *Phys. Rev. B*, **75** (2007) 125107.
[19] Karrasch, C., Pletyukhov, M., Borda, L. and Meden, V., *Phys. Rev. B*, **81** (2010) 125122.
[20] Andergassen, S., Pletyukhov, M., Schuricht, D., Schoeller, H. and Borda, L., *Phys. Rev. B*, **83** (2011) 205103; ibid. **84** (2011) 039905(E).
[21] Curzon, F.L. and Ahlborn, B., *Am. J. Phys.*, **43** (1974) 22.
[22] Van den Broeck, C., *Phys. Rev. Lett.*, **95** (2005) 190602.
[23] Schmiedl, T. and Seifert, U., *EPL*, **81** (2008) 20003.
[24] Esposito, M., Kawai, R., Lindenberg, K. and Van den Broeck, C., *Phys. Rev. Lett.*, **105** (2010) 150603.
[25] Benenti, G., Saito, K. and Casati, G., *Phys. Rev. Lett.*, **106** (2011) 230602.
[26] Yan, H. and Guo, H., *Phys. Rev. E*, **85** (2012) 011146; *Phys. Rev. E*, **86** (2012) 051135.
[27] Brandner, K., Saito, K. and Seifert, U., arXiv:1301.0492.
[28] Esposito, M., Lindenberg, K. and Van den Broeck, C., *EPL*, **85** (2009) 60010.
[29] Leijnse, M., Wegewijs, M.R. and Flensberg, K., *Phys. Rev. B*, **82** (2010) 045412.
[30] Andergassen, S., Meden, V., Schoeller, H., Splettstoesser, J. and Wegewijs, M.R., *Nanotechnology*, **21** (2010) 272001.
[31] Karrasch, C., Andergassen, S., Pletyukhov, M., Schuricht, D., Borda, L., Meden, V. and Schoeller, H., *EPL*, **90** (2010) 30003.
[32] Kennes, D.M. and Meden, V., arXiv:1210.1340.
[33] Rammer, J., *Quantum Field Theory of Non-equilibrium States* (Cambridge University Press, Cambridge, 2007).
[34] Metzner, W., Salmhofer, M., Honerkamp, C., Meden, V. and Schönhammer, K., *Rev. Mod. Phys.*, **84** (2012) 299.
[35] Entin-Wohlman, O., Imry, Y. and Aharony, A., *Phys. Rev. B*, **82** (2010) 115314.
[36] Sánchez, R. and Büttiker, M., *Phys. Rev. B*, **83** (2011) 085428.
[37] Sothmann, B. and Büttiker, M., *EPL*, **99** (2012) 27001.
[38] Doyon, B., *Phys. Rev. Lett.*, **99** (2007) 076806.
[39] For $U \neq 0$ the Landauer-Büttiker formulas for the currents can in general not be used anymore. One has to resort to the more general approach of Ref. [40]. However, in our lowest order truncation the expressions for the currents within the latter reduce (without any additional approximations) to those of the Landauer-Büttiker approach with renormalized single-particle parameters [19, 32].
[40] Meir, Y. and Wingreen, N.S., *Phys. Rev. Lett.*, **68** (1992) 2512.